engineering proceedings

MDPI

Proceeding Paper

Fault Detection on Sensors of the Quadrotor System Using Bayesian Network and Two Stage Kalman Filter †

Tolga Bodrumlu * and Fikret Çalışkan

Istanbul Technical University; caliskanf@itu.edu.tr

* Correspondence: bodrumlu@itu.edu.tr

† Presented at the 9th International Electronic Conference on Sensors and Applications, 1–15 November 2022; Available online: https://ecsa-9.sciforum.net/.

Abstract: In recent years model-based fault techniques become really popular due to reducing calculation cost. Bayesian Network and Two Stage Kalman Filter based methods have recently become quite popular due to their robustness. In this paper, model-based fault diagnosis method is presented that uses Bayesian Network and Two Stage Kalman Filter (TSKF) together to determine the sensor faults robustly in the Unmanned Aerial Vehicle (UAV) system. By using these two approaches together, the robustness of the detection of the fault in the sensor improved. For demonstrating the behavior of the proposed method, numerical simulations are performed in MATLAB/Simulink™ environment. The results show that the proposed method is capable of detecting the faults more robustly.

Keywords: unmanned aerial vehicle; two stage kalman filter; model based fault diagnosis; bayesian network

Citation: Bodrumlu, T.; Çalışkan, F. Fault Detection on Sensors of the Quadrotor System Using Bayesian Network and Two Stage Kalman Filter. *Eng. Proc.* **2022**, *4*, x. https://doi.org/10.3390/xxxxx

Academic Editor: Stefano Mariani

Published: 1 November 2022

1. Introduction

UAVs have gained a high level of popularity during the last decade in civilian, military, and engineering applications because of the recent advances in sensing, communicating, computing and controlling technologies. UAVs have several basic advantages over manned systems including increased maneuverability, reduced cost, reduced radar signatures, longer endurance, and less risk to human life. Their range are in size from full scale craft to miniature aircraft in centimeter size. These UAVs are driven by electric motors, petrol engines or gas turbines. There are lots of benefits to use UAV in different circumstances. For example, carry over to civilian aircraft that operate in hazardous conditions. Another using condition is, unmanned aircraft could carry out power line inspection in electrical cables. They are also used in, mining, detection agriculture and photographing. As an example of UAV systems, the quadrotor is a relatively simple, affordable, and easy to fly system thus it has been widely used to develop, implement and test-fly methods in control. A quadrotor is an aircraft that becomes airborne due to the lift force provided by four rotors usually mounted in cross configuration, hence its name. In this study, a quadrotor model is created based on Qball X4 quadrotor system which made by Quanser™.

Fault detection and identification is really important concept for the safety and reliability of technical processes [1–4]. Model-based fault detection techniques gain lots of popularity in recent years due to advantages of the analytical redundancy. In these approaches, there is no additional cost and weight caused by hardware redundancy [5,6]. In addition to these, there are lots of studies dealing with the fault detection algorithms for quadrotor systems. Chamseddine, Zhang, Rabbath, Fulford and Apkarian worked on actuator fault-tolerant control (FTC) for Qball-X4. Their strategy is based on Model Reference Adaptive Control (MRAC). Three different MRAC techniques which are the MIT rule

MRAC, the Conventional MRAC (C-MRAC) and the Modified MRAC (M-MRAC) have been implemented and compared with a Linear Quadratic Regulator (LQR) controller [7]. Yu, Zhang, Minchala and Qu worked on, two control algorithms based on the linear quadratic (LQ) technique of infinite time and finite time horizon applied to a quadrotor helicopter unmanned aerial vehicle (UAV) in the presence of actuator errors are applied and compared [8]. The specific control algorithms implemented are linear quadratic regulator (LQR) and model predictive control (MPC) to control the faulty and error-free quadrotor helicopter UAV test bed for both scenarios. Freddi, Longhi and Monteriù addressed the problem of fault detection and isolation (FDI) for a mini quadrotor. First a model for a four-rotor quadrotor is presented for a model obtained by a Lagrange approach. A control strategy based on PD (Proportional Derivative) controllers has been presented to stabilize quadrotor at low cruising speeds. Using Thau's observer, a diagnostic system was developed for the nonlinear model of quadrotor [9].

In this paper, a new model-based fault detection algorithm including both Bayesian Network [10] and TSKF [11] is developed. For this purpose, firstly a Bayesian Network is proposed for the estimation of possible faults in the sensors. Then a TSKF algorithm is used to detect the fault in each sensor more robustly. To estimate the fault, residuals are used. While creating the residual signal, the sensor measurements and the synthetic data obtained by adding noise to the sensor measurements are used. After the residuals are created, fault estimation is determined using the Bayesian network. Then, in order to determine fault more precisely the sensors with a high probability failure rate are inserted into the TSKF to obtain more accurate result.

The remainder of this paper is structured as follows. In Section 2, dynamics and equations of the quadrotor is given. Then the fault diagnosis algorithms presented in Section 3. In Section 4, the simulation results are presented and discussed in detail.

2. Dynamics and Equations of the Quadrocopter

2.1. Input Description

The complete dynamics of an unmanned aerial vehicle is quite complex for the control purposes. For this reason, it is interesting to consider a simplified model for the quadrotor with a minimum number of states and inputs. Although, this model includes all of the basic features that must be considered when designing control laws.

Quadrotor is controlled by the angular speeds of the four electric motors as shown in Figure 1. Each motor generates a thrust and a torque. Four control inputs as a function of torques and thrusts are defining as below:

$$\begin{aligned} u_z &= T_1 + T_2 + T_3 + T_4 \\ u_\theta &= L(T_1 - T_2) \\ u_\phi &= L(T_3 - T_4) \\ u_\psi &= \tau_1 + \tau_2 - \tau_3 - \tau_4 \end{aligned} \tag{1}$$

where u_z is the main thrust and u_θ, u_φ and u_ψ are applied pitch, roll and yaw moments, respectively. The main thrust is the sum of individual thrusts of each motor. The pitch torque is a function of the difference $T_1 - T_2$, the roll torque is a function of $T_3 - T_4$, and the yaw torque is the sum $t_1 + t_2 - t_3 - t_4$. The torque produced by each rotor is proportional to its thrust via the relation of $t_i = K_\psi T_i$ where K_ψ is the constant of proportionality.

Relation between the thrust and Pulse Width Modulation (PWM) input to each motor is approximated by a zero-order transfer function can be expressed as follows.

$$\begin{bmatrix} u_z \\ u_\theta \\ u_\phi \\ u_\psi \end{bmatrix} = \begin{bmatrix} K & K & K & K \\ KL & -KL & 0 & 0 \\ 0 & 0 & KL & -KL \\ KK_\psi & KK_\psi & -KK_\psi & -KK\psi \end{bmatrix} = \begin{bmatrix} u_1 \\ u_2 \\ u_3 \\ u_4 \end{bmatrix} \tag{2}$$

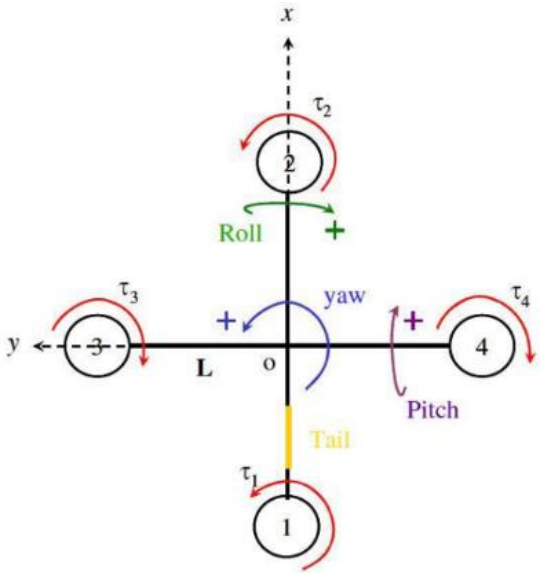

Figure 1. Schematic representation of a quadrocopter.

2.2. Quadrotor Dynamics and Equations

Using both Euler-Lagrange and Newton-Euler approach, it is possible to show that the dynamics of the quadrotor UAV can be defined as following nonlinear equations:

$$\begin{cases} m\ddot{x} = u_z(cos\,\phi\, sin\,\theta\, cos\,\psi + sin\,\phi\, sin\,\psi) \\ m\ddot{y} = u_z(cos\,\phi\, sin\,\theta\, sin\,\psi - sin\,\phi\, cos\,\psi) \\ m\ddot{z} = u_z(cos\,\phi\, cos\,\theta) - mg \\ J_1\ddot{\theta} = u_\theta \\ J_2\ddot{\phi} = u_\phi \\ J_3\ddot{\psi} = u_\psi \end{cases} \quad (3)$$

where x, y and z are the coordinates of the quadrotor UAV center of mass in the earth-frame. m: mass, θ: pitch, φ: roll, ψ: yaw. Euler angles respectively, and J_i (i = 1, 2, 3) are the moments of inertia along y, x, and z directions, respectively

Table 1. Parameters Table [12].

Symbol	Explanation	Value
K	Thrust Gain	120 N
L	Distance from motor to center of gravity	0.2 m
K_φ	Thrust to moment gain	4 N·m
M	Mass	1.4 kg
G	Gravitational acceleration	9.81 m/s^2
J_1; J_2; J_3	Moments of Inertia	0.03; 0.03; 0.04 kg·m^2

2.3. Linearization and State Space Description

In order to linearize the nonlinear Equations (3), it will fix around an equilibrium point. The state variables are defined as follows:

$$\underset{\sim}{x} = [x_1x_2x_3x_4x_5x_6x_7x_8x_9x_{10}x_{11}x_{12}]^T = [x\dot{x}y\dot{y}z\dot{z}\theta\dot{\theta}\varphi\dot{\varphi}\psi\dot{\psi}]^T \quad (4)$$

that underline means the vector form. In addition to that, to define the equation in the linear state space form a nominal point is needed. Moreover, assuming that the quadrotor stays in predefined position with no yawing and small roll and pitch angles. Then, the nominal inputs are as shown:

$$[\tilde{u}_z \tilde{u}_\theta \tilde{u}_\phi \tilde{u}_\psi]^T = [mg000]^T \tag{5}$$

where "~" denotes the nominal value and g is the gravitational acceleration. Linearized state space A, B, C and D matrices are the Jacobian matrices calculated at the nominal points.

$$\begin{aligned} \dot{\underline{x}} &= A\underline{x} + B\underline{u} \\ \underline{y} &= C\underline{x} + D\underline{u} \end{aligned} \tag{6}$$

$$A = \frac{\partial f}{\partial x}(\tilde{\underline{x}}, \tilde{\underline{u}}, t), B = \frac{\partial f}{\partial u}(\tilde{\underline{x}}, \tilde{\underline{u}}, t), C = I_{12x12}, D = 0_{12x4} \tag{7}$$

that I and 0 are the Identity and Zero matrices respectively. Let u_i (PWM inputs to propellers) as inputs to the system using (2), (3), (4) linearized state space matrices become

$$A = \begin{bmatrix} 0 & 1 & 0 & 0 & 0 & 0 & 0 & 0 & 0 & 0 & 0 & 0 \\ 0 & 0 & 0 & 0 & 0 & 0 & g & 0 & 0 & 0 & 0 & 0 \\ 0 & 0 & 0 & 1 & 0 & 0 & 0 & 0 & 0 & 0 & 0 & 0 \\ 0 & 0 & 0 & 0 & 0 & 0 & 0 & 0 & -g & 0 & 0 & 0 \\ 0 & 0 & 0 & 0 & 0 & 1 & 0 & 0 & 0 & 0 & 0 & 0 \\ 0 & 0 & 0 & 0 & 0 & 0 & 0 & 0 & 0 & 0 & 0 & 0 \\ 0 & 0 & 0 & 0 & 0 & 0 & 0 & 1 & 0 & 0 & 0 & 0 \\ 0 & 0 & 0 & 0 & 0 & 0 & 0 & 0 & 0 & 0 & 0 & 0 \\ 0 & 0 & 0 & 0 & 0 & 0 & 0 & 0 & 0 & 1 & 0 & 0 \\ 0 & 0 & 0 & 0 & 0 & 0 & 0 & 0 & 0 & 0 & 0 & 0 \\ 0 & 0 & 0 & 0 & 0 & 0 & 0 & 0 & 0 & 0 & 0 & 1 \\ 0 & 0 & 0 & 0 & 0 & 0 & 0 & 0 & 0 & 0 & 0 & 0 \end{bmatrix}, \tag{8}$$

$$B = \begin{bmatrix} 0 & 0 & 0 & 0 \\ 0 & 0 & 0 & 0 \\ 0 & 0 & 0 & 0 \\ 0 & 0 & 0 & 0 \\ 0 & 0 & 0 & 0 \\ \frac{K}{m} & \frac{K}{m} & \frac{K}{m} & \frac{K}{m} \\ 0 & 0 & 0 & 0 \\ \frac{KL}{J_1} & \frac{-KL}{J_1} & 0 & 0 \\ 0 & 0 & 0 & 0 \\ 0 & 0 & \frac{KL}{J_2} & \frac{-KL}{J_2} \\ 0 & 0 & 0 & 0 \\ \frac{KK_\psi}{J_3} & \frac{KK_\psi}{J_3} & \frac{-KK_\psi}{J_3} & \frac{-KK_\psi}{J_3} \end{bmatrix}, \tag{9}$$

Since, this study is based on discrete time domain, state space

$$\begin{aligned} A_k = e^{ATs}, B_k = \int_0^{Ts} e^{A\tau} d\tau B \\ C_k = I_{12x12}, D_k = 0_{12x4} \end{aligned} \tag{10}$$

In the next section fault diagnosis algorithm is explained in detail. Firstly, Bayesian Network is explained. After the Bayesian Network explanation, the Kalman Filter and its equations are given.

3. Fault Diagnosis

3.1. Fault Detection Using Bayesian Network

In this part of the study, Bayesian Network is explained in general terms. The joint distribution of the Bayesian network is calculated using the chain rule [10]:

$$P(A_1, A_2, \dots, A_n) = \prod_{i=1}^{n} P(A_i | A_1, ., ., A_{i-1}) \quad (11)$$

where $P(A_1, A_2, \dots, A_n)$ is the joint distribution of all the variables, A_i is the child node and $A_1, \dots, A_{i-1}$ are the parents of the child node. The joint distribution of all the variables is equal to the product of each child A_i with its parent nodes $A_1, \dots, A_{i-1}$. The marginalization of the joint probability distribution over the variables is given by (12) below:

$$P(A_1, A_2) = \sum_{\forall a_3 \in A_3} P(A_1, A_2, A_3) \quad (12)$$

Using Equations (11) and (12), and considering the conditional probability between each variable, fault diagnosis with Bayesian networks can be realized. Developing the conditional probability distributions (CPD) between the nodes are required to determine both the relationship between the nodes in the structure and to reflect the confidence in each value obtained from the node [10]. Within the generated structure shown in Figure 2, each residual has its own CPD. To further demonstrate the association between CPDs and Bayesian network, consider the example network shown in Figure 3. In this case, each event and the outcome take on binary values, which can be thought of as a fault either being present or absent. Given two events A and B, by definition the conditional probability of A given B is:

$$P(A|B) = \frac{P(A, B)}{P(B)} \quad (13)$$

In Figure 3, the structure of the residuals with Bayesian Network has shown.

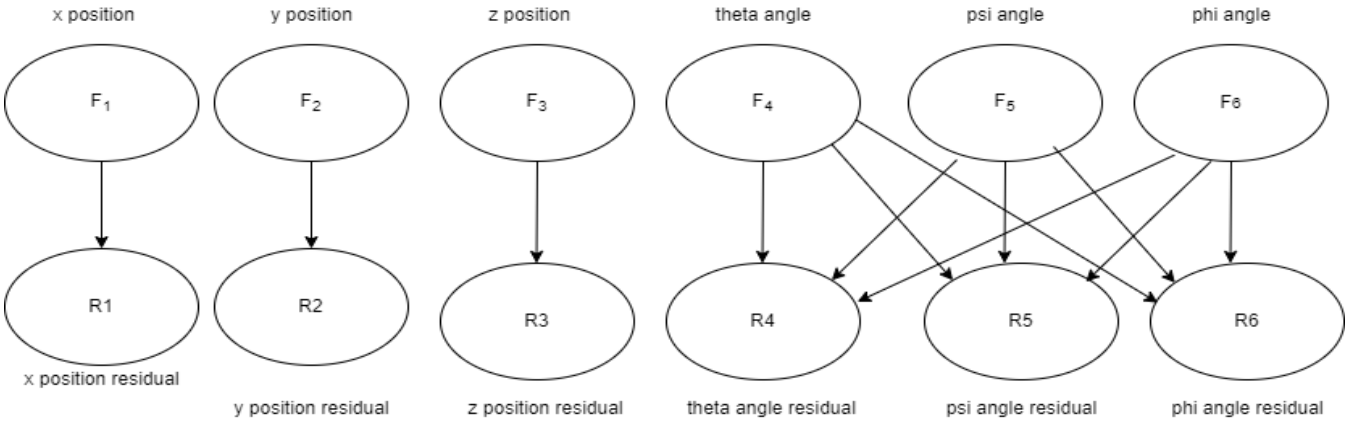

Figure 2. The structure of the residuals.

As it can be seen from the Figure 3, a model has been constructed in which the roll and pitch angles are dependent on each other, and the positions (x, y and z) are independent of each other. In this Bayesian Network, default values are set for false positive and false negative results. These are 0.1 ($\Lambda_p = 0.1$) and 0.05 ($\Lambda_n = 0.05$), respectively. After setting these values, a threshold value is determined for each residual. Determination of this residual values threshold is explained in detailly in the Section 4. Using the CPD tables and residual values, a Bayesian Network structure is created. Determination of the fault based on whether the fault probability exceeds this threshold or not. In the next section, equation of the TSKF is explained. In addition to that, how fault detection is made more robust is mentioned.

3.2. Fault Detection Using Kalman Filter

When looking at the Bayesian Network, it is seen that it is so difficult to distinguish sensor fault from each other, especially when a fault occurs in the psi and theta sensors. Because these angle values are coupled with each other. A fault in one affects the other. For this reason, the sensor values with a high probability of fault will be given to the Kalman Filter, and it will be possible to determine whether there is a malfunction in that sensor. The first of the most important advantage is fault identification will do more precisely and there will be no problem in terms of calculation cost by running the TSKF since only the high probability of failure value sensor are using.

In this section, TSKF is used for the fault detection algorithm. A discrete linear time-varying state-space model is used to describe dynamic system as following [11]:

$$\begin{aligned} x_{k+1} &= A_k x_k + B_k u_k + w_k{}^x \\ y_{k+1} &= C_k x_{k+1} + v_{k+1} \end{aligned} \tag{14}$$

where $x_k \in R^n$, $u_k \in R^l$ and $y_{k+1} \in R^m \in$ are the state, control input and output variables, respectively. $W_k{}^x$ and v_{k+1} are uncorrelated Gaussian random vectors with zero means and covariance matrices $Q_x{}^k$ and R_k, respectively. The bias augmented discrete linear state-space model is written as:

$$\begin{aligned} x_{k+1} &= A_k x_k + B_k u_k - B_k U_k \gamma_k + w_k{}^x \\ \gamma_{k+1} &= \gamma_k + w_k{}^\gamma \\ \gamma_{k+1} &= C_k x_{k+1} + v_{k+1} \end{aligned} \tag{15}$$

The optimal bias estimator written as follows:

$$\begin{aligned} &\hat{\gamma}_{k+1|k} = \hat{\gamma}_{k|k} \\ &P^{\gamma}_{k+1|k} = P^{\gamma}_{k|k} + Q^{y}_{k} \\ &\hat{\gamma}_{k+1|k+1} = \hat{\gamma}_{k+1|k} + K^{\gamma}_{k+1}\left(\bar{r}_{k+1} - H_{k+1|k}\hat{\gamma}_{k|k}\right) \\ &K^{\gamma}_{k+1} = P^{\gamma}_{k+1|k} H_{k+1|k} (H_{k+1|k} P^{\gamma}_{k+1|k} H^T{}_{k+1|k} + \bar{S}_{k+1})^{-1} \\ &P^{\gamma}_{k+1|k+1} = (I - K^{\gamma}_{k+1} H_{k+1|k}) P^{\gamma}_{k+1|k} \end{aligned} \tag{16}$$

The Bias-free state estimator can be expressed as follows:

$$\begin{aligned} &\tilde{x}_{k+1|k} = A_k \tilde{x}_{k|k} + B_k u_k + W_k \hat{\gamma}_{k|k} - V_{k+1|k} \hat{\gamma}_{k|k} \\ &\tilde{P}^{x}_{k+1|k} = A_k \tilde{P}^{x}_{k|k+} A^T_k + Q^x_k + W_k P^{\gamma}_{k|k} W^T_k - V_{k+1|k} P^{\gamma}_{k+1|k} V^T{}_{k+1|k} \\ &\tilde{x}_{k+1|k+1} = \tilde{x}_{k+1|k} + \tilde{K}^{x}_{k+1}\left(y_{k+1} - C_{k+1}\tilde{x}_{k+1|k}\right) \\ &\tilde{K}^{x}_{k+1} = \tilde{P}^{x}_{k+1|k} + C^T_{k+1}(C_{k+1}\tilde{P}^{x}_{k+1|k} C^T_{k+1} + R_{k+1})^{-1} \\ &\tilde{P}^{x}_{k+1|k+1} = (I - \tilde{K}^{x}_{k+1} C_{k+1}) \tilde{P}^{x}_{k+1|k} \end{aligned} \tag{17}$$

The filter residual and covariance equations written as below.

$$\begin{aligned} \tilde{r}_{k+1} &= y_{k+1} - C_{k+1}\tilde{x}_{k+1|k} \\ \tilde{S}_{k+1} &= C_{k+1}\tilde{P}^{x}_{k+1|k} C^T_{k+1} + R_{k+1} \end{aligned} \tag{18}$$

The coupling equations can be expressed as below

$$\begin{aligned} &W_k = A_k V_{k|k} - B_k U_k \\ &V_{k+1|k} = W_k P^{\gamma}_{k|k} (P^{\gamma}_{k+1|k})^{-1} \\ &H_{k+1|k} = C_{k+1} V_{k+1|k} \\ &V_{k+1|k+1} = V_{k+1|k} - \tilde{K}^{x}_{k+1} H_{k+1|k} \end{aligned} \tag{19}$$

The compensated error and covariance estimator written as:

$$\hat{x}_{k+1|k+1} = \tilde{x}_{k+1|k+1} + V_{k+1|k+1}\hat{y}_{k+1|k+1}$$
$$P_{k+1|k+1} = \tilde{P}^{x}_{k+1|k+1} + V_{k+1|k+1}P^{y}_{k+1|k+1} + V^{T}_{k+1|k+1} \quad (20)$$

The block diagram of TSKF, whose equations are given, is given below (Figure 3). In the next section, simulation results will be explained.

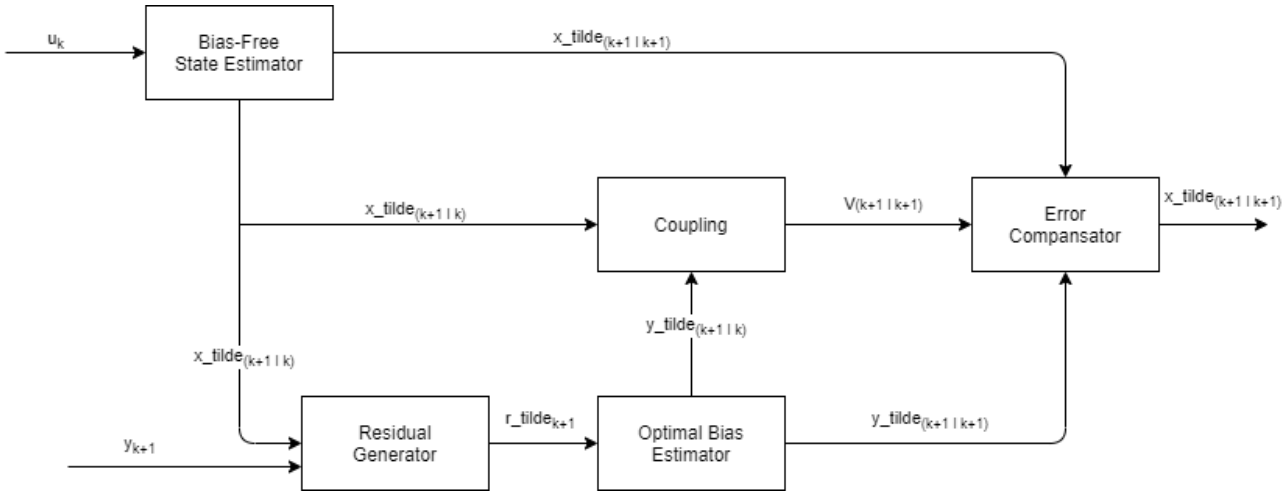

Figure 3. TSKF Block Diagram.

4. Simulation System and Results

4.1. Simulation System

The fault diagnosis algorithm is tested by using the synthetic data. This data created in the Simulink™ environment. The Bayesian Network and TSKF structure implemented in the Simulink environment. Figure 3 illustrate the model block diagrams for the quadrotor equations, TSKF and Bayesian Network respectively.

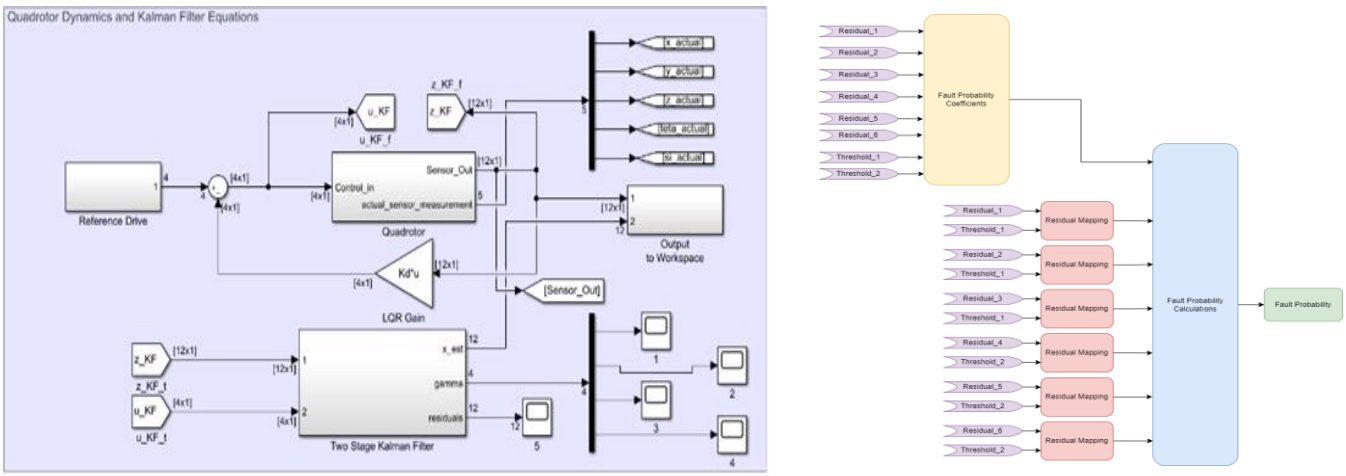

Figure 4. Quadrotor System and TSKF Equations.

4.2. Results and Discussion

The results are generated using the simulation system described in the previous section. The first of the results obtained are residual values of each sensor. This is shown in Figure 5 below.

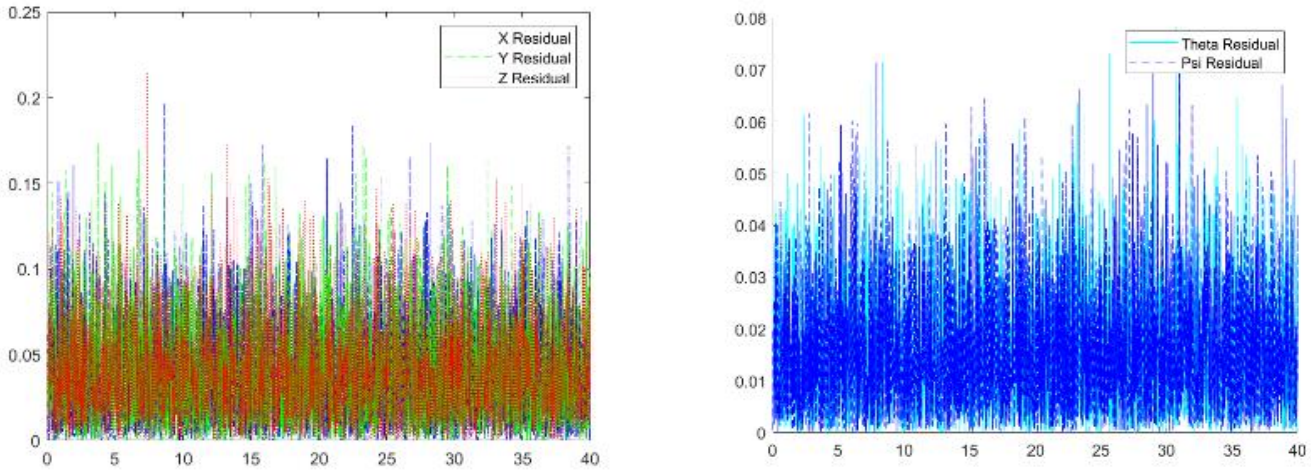

Figure 5. Residual Values for the sensors.

As shown in Figure 5, it is seen that x, y and z values are close to each other and theta and psi values are close to each other. The maximum value of the calculated residual values is chosen 0.25 for x, y and z values. For the theta and psi angle, the maximum threshold values are 0.08. Since it is assumed that there is no malfunction in the system, the threshold value for each residual is determined to 0.25 for x, y, z and 0.08 for theta and psi, respectively.

Test Cases

The test case results are generated using the simulation system described in the previous section

(a) No Fault

When there is no malfunction in the system, it can be easily seen from the Figure 6 that the probability of failure calculated with Bayesian Network is quite small.

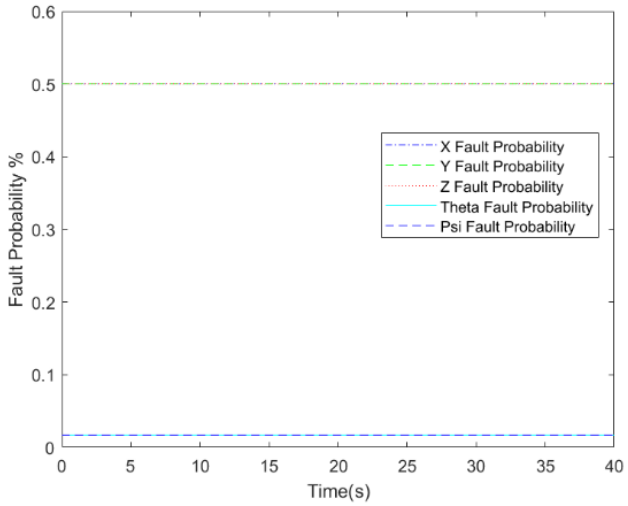

Figure 6. Bayesian Fault Probability (No Fault).

(b) Theta Angle Sensor Fault

In cases where the residual values of R_4 and R_5 exceed the threshold value which shown in Table 2, it can be detected that there is a fault in the theta and psi angle when we look at Figure 7. However, only theta angle sensor is manually faulted between 20–30 s. Since this situation cannot be distinguished by the Bayesian Network, the faulty sensors inserted into the TSKF, and it can be easily understood by looking at the Figures 8–10 that theta sensor is really faulty.

Table 2. Residual Threshold Values.

Residual	Threshold Value
R_1, R_2, R_3	0.25
R_4, R_5	0.08

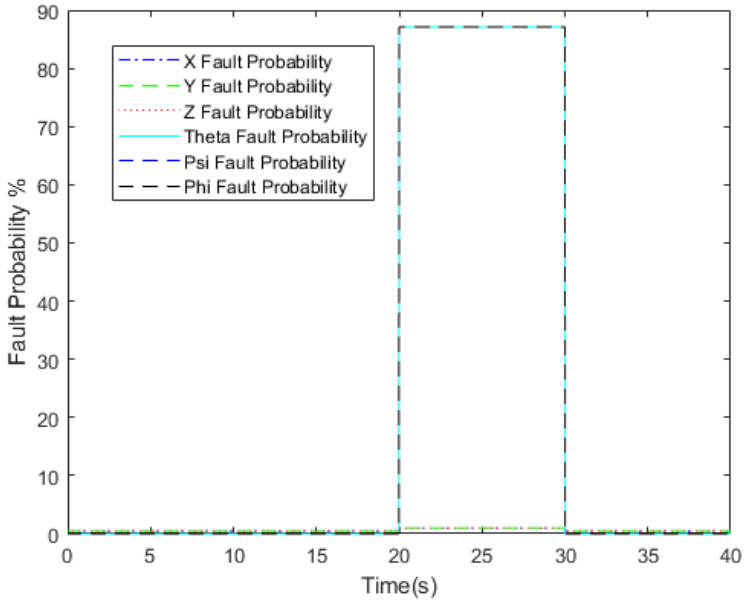

Figure 7. Bayesian Fault Probability (Theta Angle Fault).

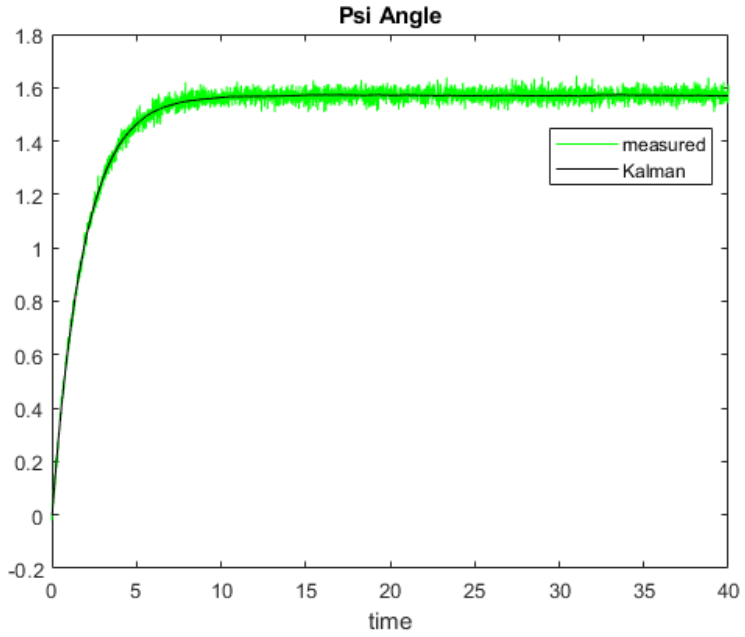

Figure 8. Psi Angle Measured and Kalman Value.

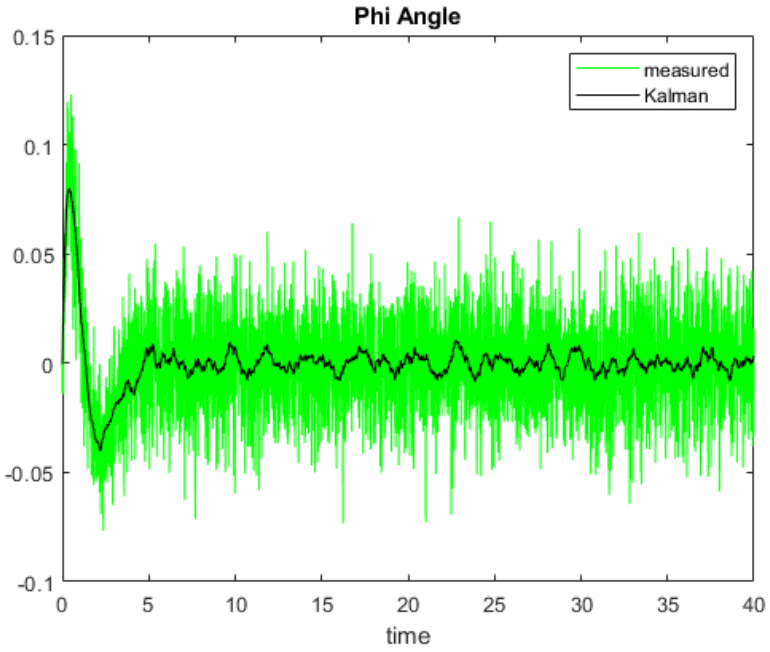

Figure 9. Phi Angle Measured and Kalman Value.

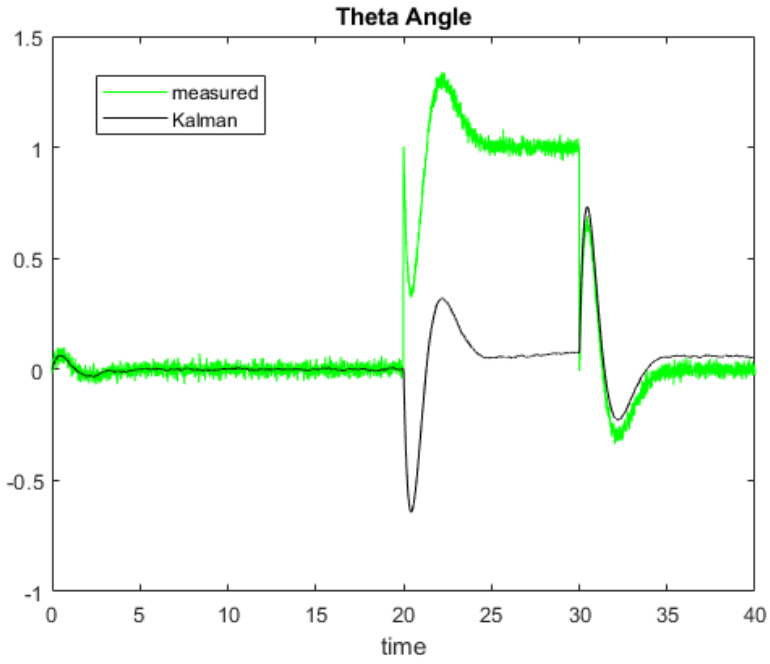

Figure 10. Theta Angle Measured and Kalman Value.

5. Conclusions

In this paper, a model-based fault diagnostic method is presented which is capable of determining the faults using both Bayesian Network and TSKF. With the Bayesian Network, it was possible to detect which sensors are faulty. Although, since some sensors are coupled with each other, there are some cases where the faults cannot be separated. At this point, fault detection can be performed more accurately by using TSKF structure described in this study. In addition, this TSKF structure provides a computational gain because it works only for sensors that are detected as faulty with Bayesian Network.

The implementation of the fault detection structure is carried out using synthetic test data and tests of the algorithm are done in MATLAB/Simulink environment. The results

show us that, the fault detection algorithm is able to detect the corresponding faults correctly when the residuals are manually triggered. In addition, it gives precise results by using Bayesian and TSKF together. In the future, it is aimed to collect real test data and to make the threshold values more robust.

Author Contributions:

Funding: This research was financially supported by Istanbul Technical University, grant number 42754.

Institutional Review Board Statement: Not applicable.

Informed Consent Statement: Not applicable.

Data Availability Statement: Not applicable.

Conflicts of Interest: The authors declare no conflict of interest.

References

1. Patton, R.J. Robust model-based fault diagnosis: the state of the art. In Proceedings of the IFAC Symposium on Fault Detection, Supervision and Safety for Technical Processes (SAFEPROCESS'94), Espoo, Finland, 13–16 June 1994, pp. 69–74.
2. Isermann, R. Model-based fault-detection and diagnosis-status and applications. *Annu. Rev. Control.* 2005, 29, 71–85.
3. Frank, P.M.; Ding, X. Freqeuncy Domain Approach to Optimally Robust Residual Generation and Evaluation for Model-Based Fault Diagnosis. *Automatica* **1994**, *30*, 789–804.
4. Zhong, M.; Xue, T.; Ding, X. A survey on model-based fault diagnosis for linear discrete time-varying systems. *Neurocomputing* **2018**, *306*, 51–60.
5. Ding, S.X. *Model-based Fault Diagnosis Techniques: Design Schemes, Algorithms, and Tools*; Springer: Berlin, Germany, 2008.
6. Marzat, J.; Lahanier, H.P.; Damongeot, F.; Walter, E. Model-based fault diagnosis for aerospace systems: a survey. *Proc. Inst. Mech. Eng. Part G J. Aerosp. Eng.* **2011**, *226*, 1329–1360.
7. Chamseddine, A.; Zhang, Y.; Rabbath, C.-A.; Apkarian, J.; Fulford, C. Model Reference Adaptive Fault Tolerant Control of a Quadrotor UAV. In Proceedings of the AIAA Infotech at Aerospace Conference and Exhibit 2011, St. Louis, MO, USA, 29–31 March 2011. https://doi.org/10.2514/6.2011-1606
8. Yu, B.; Zhang, Y.; Minchala, I.; Qu, Y. Fault-tolerant control with linear quadratic and model predictive control techniques against actuator faults in a quadrotor UAV. In Proceedings of the 2013 Conference on Control and Fault-Tolerant Systems (SysTol), Nice, France, 9–11 October 2013; pp. 661–666
9. Freddi, A.; Longhi, S.; Monteriù, A. Actuator fault detection system for a mini-quadrotor. In Proceedings of the 2010 IEEE International Symposium on Industrial Electronics, Bari, Italy, 4–7 July 2010; pp. 2055–2060
10. Cai, B.; Huang, L.; Xie, M. Bayesian Networks in Fault Diagnosis. *IEEE Trans. Ind. Inform.* **2017**, *13*, 2227–2240.
11. Amoozgar, M.H.; Chamseddine, A.; Zhang, Y. Experimental Test of a Two-Stage Kalman Filter for Actuator Fault Detection and Diagnosis of an Unmanned Quadrotor Helicopter. *J. Intell. Robot. Syst.* **2012**, *70*, 107–117.
12. Bodrumlu, T.; Soylemez, M.T.; Mutlu, I. Modelling and Control of the Qball X4 Quadrotor System Based on PID and Fuzzy Logic Structure. In Proceedings of the 13th European Workshop on Advanced Control and Diagnosis (ACD 2016), Lille, France, 17–18 November 2016; Volume 783.